NANO LETTERS

Letter

pubs.acs.org/NanoLett

Broadly Defining Lasing Wavelengths in Single Bandgap-Graded Semiconductor Nanowires

Zongyin Yang,[†,¶,§] Delong Wang,[†,⊥,§] Chao Meng,[†] Zhemin Wu,[‡] Yong Wang,[‡] Yaoguang Ma,[∥] Lun Dai,[∥] Xiaowei Liu,[†] Tawfique Hasan,[¶] Xu Liu,[†] and Qing Yang*[,†]

[†]State Key Laboratory of Modern Optical Instrumentation, Department of Optical Engineering, Zhejiang University, Hangzhou 310027, China

[⊥]National Laboratory of Solid State Microstructures and College of Engineering and Applied Sciences, Nanjing University, Nanjing 210093, China

[‡]Center of Electron Microscopy and State Key Laboratory of Silicon Materials, Department of Materials Science and Engineering, Zhejiang University, Hangzhou 310027, China

[∥]State Key Lab for Mesoscopic Physics and School of Physics, Peking University, Beijing 100871, China

[¶]Cambridge Graphene Centre, University of Cambridge, Cambridge CB3 0FA, United Kingdom

Supporting Information

ABSTRACT: Designing lasing wavelengths and modes is essential to the practical applications of nanowire (NW) lasers. Here, according to the localized photoluminescence spectra, we first demonstrate the ability to define lasing wavelengths over a wide range (up to 119 nm) based on an individual bandgap-graded CdSSe NW by forward cutting the NW from CdSe to CdS end. Furthermore, free spectral range (*FSR*) and modes of the obtained lasers could be controlled by backward cutting the NW from CdS to CdSe end step-by-step. Interestingly, single-mode NW laser with predefined lasing wavelength is realized in short NWs because of the strong mode competition and increase in *FSR*. Finally, the gain properties of the bandgap-graded NWs are investigated. The combination of wavelength and mode selectivity in NW lasers may provide a new platform for the next generation of integrated optoelectronic devices.

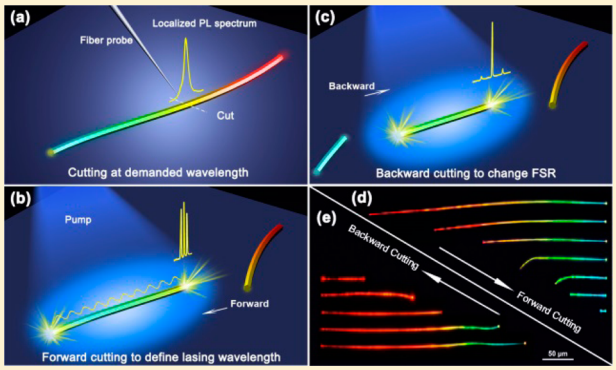

KEYWORDS: *Cadmium Sulfide Selenide, Bandgap-Graded Nanowire, Lasing, Defining Wavelength, Mode Selectivity*

Semiconductor NW lasers have recently attracted a great deal of interest because they have a large number of potential applications in future photonic and optoelectronic devices.[1−5] To push NW lasers closer to practical applications, some important challenges, for instance, wavelength variability, must be addressed. To date, a number of binary semiconductor NW lasers with discrete wavelengths ranging from ultraviolet to near-infrared have been reported.[6−15] Besides the discrete wavelength lasers, wavelength continuously variable lasers are specifically required in many situations, such as saturated spectroscopy,[16] environmental monitoring,[17] and optical communication,[18] and so forth.

To achieve wavelength continuously variable NW lasers, recent research works have successfully demonstrated with two routes: designing new cavities or utilizing new gain media. With regard to new cavity design, wavelength tunability through changing the geometry of the cavity by micromanipulation has been reported.[19] Unfortunately, the tuning range is limited to less than 10 nm for a single NW, which is insufficient for many applications. As for new gain media, some novel materials have been synthesized, such as multi-quantum-well NW heterostructures[20] and homogeneous ternary alloy NWs[21] and nanoribbons,[22,23] which have made important contributions to the enrichment of lasing wavelengths. However, the wavelength variability is realized by employing several NWs with different bandgaps rather than single, identical NWs. Precise controlling of the composition and multiple growth batches are needed in order to achieve different composite NWs. Recently, intrinsic self-absorption and Burstein−Moss effect were introduced to tailor the single undoped NW lasing wavelengths continuously variable for 30−40 nm spectral range,[24−26] which is a simple and effective approach but is limited by the gain profile of the NW. The emergence of individual spatial bandgap-graded semiconductor NWs offers the possibility of realizing ultrawide wavelength tunable light emitting devices, high-performance field-effect transistors, and

Received: February 3, 2014
Revised: April 30, 2014
Published: May 5, 2014

high-efficiency solar cells in identical NWs.[27−30] Very recently, multicolor lasing is realized from a single bandgap-graded CdSSe nanoribbon by multiscattering effect at morphology defect sites of the nanoribbon.[31] However, the lasing wavelength is difficult to control and tune because of the random distribution of the defects.

In this paper, we demonstrate a novel approach to define NW laser wavelengths and modes over a wide spectral range in individual bandgap-graded CdSSe NWs using a combination of new gain material and new cavity design. The range of lasing wavelengths from a single NW could cover more than 119 nm. With further optimization of material growth, the wavelength tuning range can be eventually extended to around 200 nm. Interestingly, we find the lasing wavelengths can be well defined by the center wavelength of the photoluminescence (PL) from the NW narrow-bandgap end. Therefore, it is convenient to get the desired lasing wavelengths according to the localized PL spectrum when producing a NW laser. Furthermore, the *FSR* of these achieved NW lasers could be controlled with small wavelength fluctuation of dominant peaks. On the basis of these results, a single mode laser with precise wavelength definition has also been realized. To the best of our knowledge, there are no reports on controlling wavelengths in combination with modes over such a wide spectral range in single semiconductor NW lasers. The gain properties of these NWs are also investigated, which may give a better understanding of lasing mechanism in such particular NWs.

Figure 1 presents the schematic diagram of our approach. The bandgap-graded CdSSe NWs used in this work are synthesized by the source-moving chemical vapor deposition (CVD) method that has been described in our previous work.[27] Along the growth direction of as-fabricated bandgap-graded CdSSe NW, the composition is continuously tuned from CdS at one end to CdSe at the other end (Supporting Information Figure S1), resulting in the corresponding bandgap (also the light emission wavelength) to be modulated gradually from 2.44 eV (507 nm, green light) to 1.74 eV (710 nm, red light). Although each section with a different emission color could be served as gain material in one Fabry−Pérot (FP) cavity formed by NW's end-facets, only the longest lasing wavelength can be observed due to the asymmetric light propagation effect.[32] In order to make full use of the emission colors, the narrow-bandgap end with longest emission wavelength could be cut off to form a new NW cavity where the lasing wavelength is controlled by the new narrow-bandgap end. As shown in Figure 1a, the cut point is selected according to the NW's localized PL spectrum and then the NW is cut by a homemade fiber probe into two different segments: segment I for wide-bandgap segment and segment II for narrow-bandgap segment. Figure 1b illustrates the lasing process when pumping the segment I. The lasing wavelength is defined by the localized PL center wavelength of the cut point. Moreover, as shown in Figure 1c, the *FSR* of the laser can be controlled by the backward cutting process with small shift in the dominant lasing wavelength.

The NWs are transported from the as-grown substrate to a MgF_2 substrate for micromanipulation and optical characterization. Generally, the as-synthesized NWs have diameters of 100−1000 nm and lengths of up to 500 μm.[27] Using a simple bend-to-fracture method,[33,34] we can cut a NW easily along its *c* axis at a predetermined point, as shown in Figure 2a. This method could ensure relatively perfect end-facets (Figure 2b) and, thus, provide high-quality FP resonators. The NW is excited by a 355 nm pulsed laser obtained from a frequency-

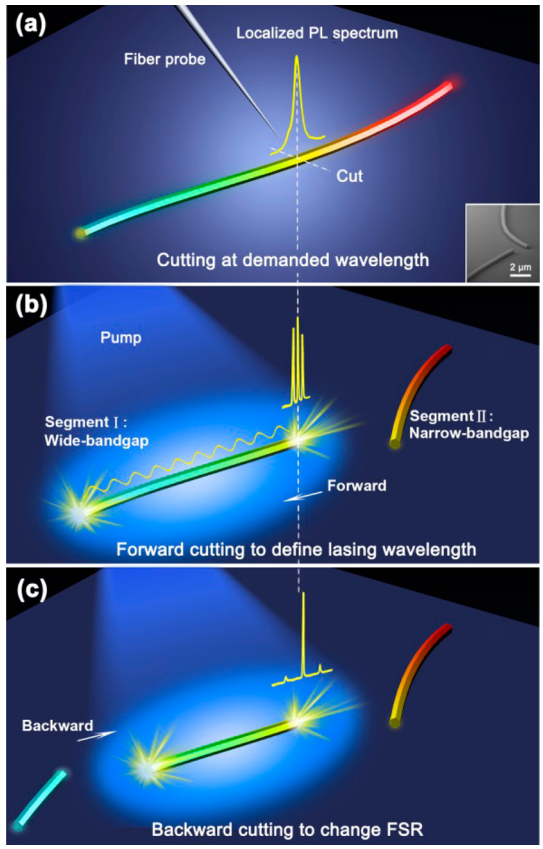

Figure 1. Schematic diagram of the approach to control wavelengths in combination with modes in NW laser. (a) Sketch of selecting the cut point according to the localized PL spectrum. Inset: scanning electron microscope image of a NW which is cut at a selected point. (b) Laser emission at the demanded wavelength after cutting the NW at the selected point into two segments and pumping the segment I: wide-bandgap segment. By cutting the NW in forward direction step-by-step, continuously variable lasing wavelengths could be obtained. (c) Designing *FSR* by backward cutting.

tripled Nd:YAG laser (10 kHz, 10 ns pulse width), which is coupled to a silica fiber to excite the NW from the side. The silica fiber is attached to a three-dimensional translation stage for precisely controlling the pump area (with a largest diameter of 250 μm, Supporting Information Figure S2). In our experiments, it is found that the pump area has no obvious influence on the emission lasing wavelength (see Supporting Information Figure S5). The emission light is collected by a 100× lens at the narrow-bandgap end using our micro-PL spectrum mapping setup with a spatial resolution of ∼3 μm while the PL image is captured using a 20× lens in order to observe the whole NW at one time. A real-color PL image of a typical NW at low pump density is shown in Figure 2c, which exhibits a gradual color change from green to red, indicating a good bandgap-graded property along the NW *c* axis. Emission spectrum collected from the left narrow-bandgap end of the NW is centered at 638 nm with a full width at half-maximum (FWHM) of 30 nm (Figure 2e, bottom). With increasing pump density, bright red spots emerged at both ends of the NW (Figure 2d), and the measured spectrum from the same left end exhibits a sharp lasing line at 639 nm (Figure 2e, top). Supporting Information Figure S3 shows that the lasing spectra measured from two ends of a NW have the same center wavelength. The only difference between them is that the

dx.doi.org/10.1021/nl500432m | *Nano Lett.* 2014, 14, 3153−3159

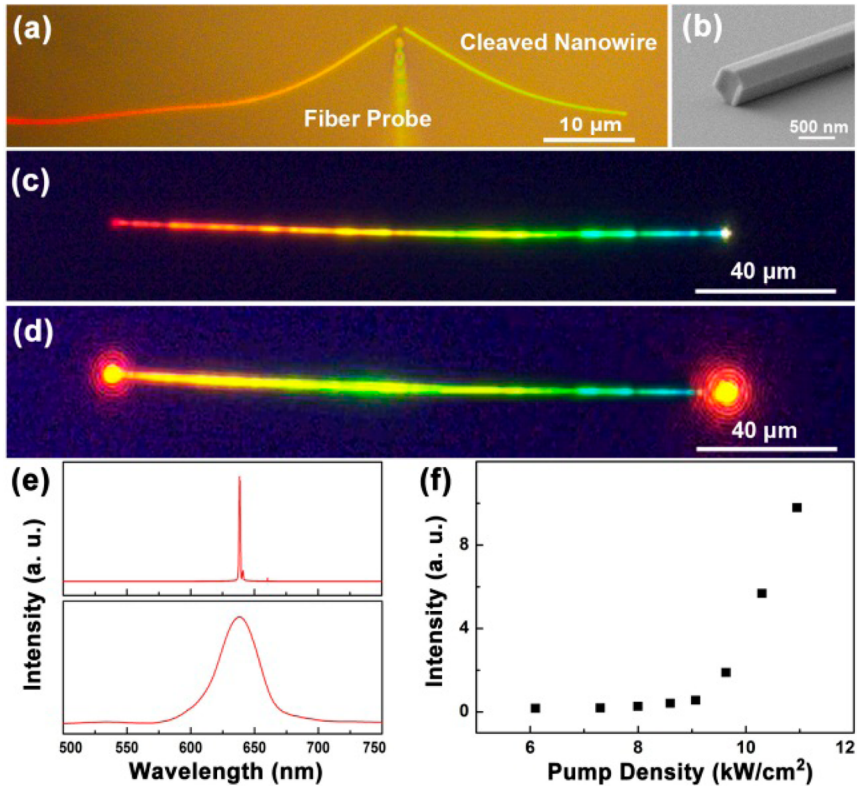

Figure 2. Micromanipulation and optical measurements of bandgap-graded NWs. (a) Optical microscope image of a NW being cut by a fiber probe. (b) Scanning electron microscope image of one endfacet of the cleaved NW shown in (a). (c, d) Real-color optical microscope images of a NW with a diameter of ~500 nm and length of ~170 μm under low and high pump density, respectively. (e) Spontaneous emission spectrum (bottom) and lasing spectrum (top) collected from the left end of the same NW as in (c) and (d), respectively. (f) Integrated output power as a function of pump density.

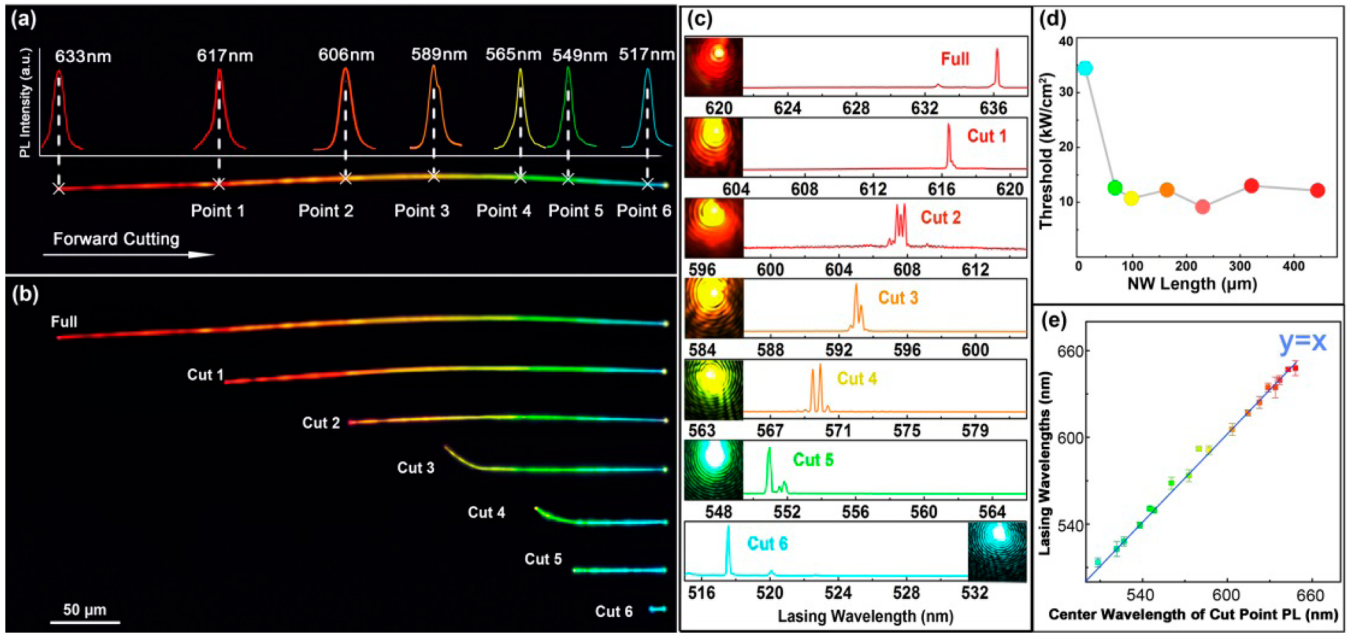

Figure 3. Defining lasing wavelengths over a wide range on an individual bandgap-graded NW. (a) Real-color image of a bandgap-graded NW with six cut points determined by localized PL spectra. The NW has a diameter of ~450 nm and a length of 435 μm. (b) Real-color images of the NW after being cut at point 1 to point 6 sequentially. (c) Lasing spectra obtained from NW full to cut 6 are shown in (b). The colorful spots shown in each spectrum correspond to the real color image of the end emission of each NW at pump density above threshold. (d) Lasing threshold versus NW length of NW full to cut 6. (e) Lasing wavelengths versus PL center wavelengths measured from five bandgap-graded NWs and each NW is cut step-by-step for variable wavelength lasing emission. Colorful rectangles, experimental data; blue line, function $y = x$ as a guide.

dx.doi.org/10.1021/nl500432m | *Nano Lett.* 2014, 14, 3153−3159

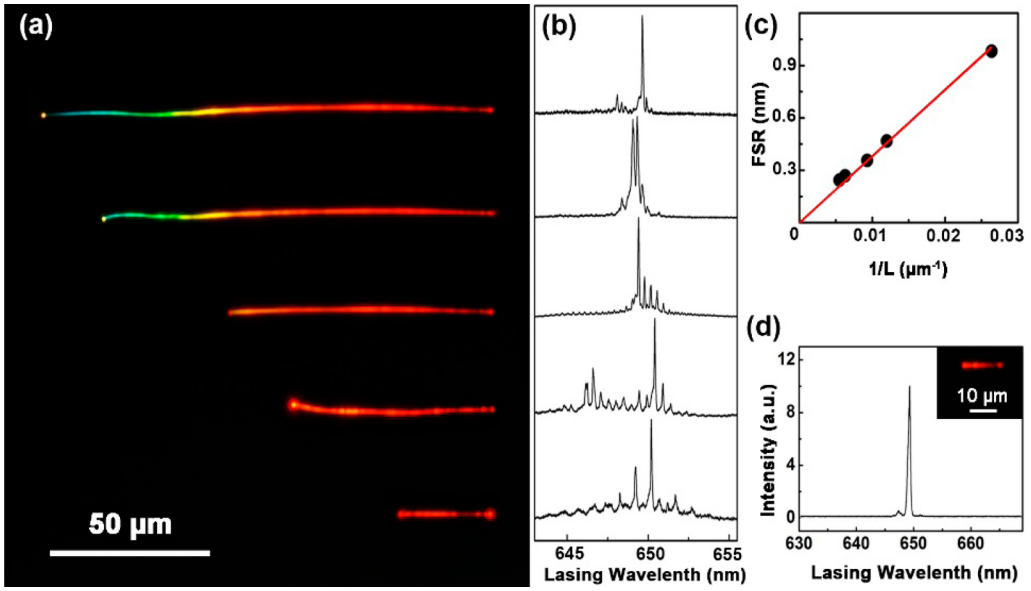

Figure 4. Optical characterization of a NW (~450 nm in diameter, 180 μm in length) cut by backward cutting. (a) Real color images of the NW after being cut at different points. (b) The corresponding lasing spectra of the cut NW in (a). (c) *FSR* versus inverse NW length 1/*L*. (d) Output spectrum of a single-mode laser. Inset: real color image of the NW.

spectrum from the wide-bandgap end contains less PL background. To further confirm the laser oscillation, integrated output power versus pump density was recorded, as illustrated in Figure 2f, which clearly shows a lasing threshold of ~9 kW/cm^2.

Here, we demonstrate the ability to define lasing wavelengths over a wide range using an individual bandgap-graded CdSSe NW. The NW has a diameter of ~450 nm and a length of ~435 μm. The measured center wavelength of the PL is from 507 nm at right end (wide-bandgap end) to 633 nm at left end (narrow-bandgap end, Figure 3a). We can specially tailor lasing wavelengths by forward cutting the NW according to the mechanism shown in Figure 1b. If we want to fabricate, for instance, a NW laser operating at λ = 617 nm, we need only to perform the following experimental procedure. First, find the point on the NW where the PL center wavelength is about 617 nm at low pump density by our micro-PL spectrum mapping measurements setup (see Supporting Information Figure S2). Second, cut the NW at the point into two segments and excite segment I with increasing pump density until the buildup of the lasing action (Figure 1b). As shown in Figure 3c (cut 1), the measured laser emission wavelength is 616.5 nm, which is well consistent with the PL center wavelength. Similarly, five other specific points on the NW (from point 2 to point 6) are randomly selected, the localized PL center wavelengths of which are 606, 589, 566, 549, and 517 nm with FWHM of 30 nm, respectively, as shown in Figure 3a. The corresponding lasing wavelengths of 607.5, 593, 570, 553, and 517.5 nm are achieved when the NW is cut at these points sequentially (Figure 3c, cut 2 to cut 6). The small red shifts of the lasing wavelength compared with the PL center wavelength is attributed to the wide FWHM of the PL and slight self-absorption. The results clearly demonstrate the ability to control lasing wavelengths over a wide range in an individual bandgap-graded NW.

Utilizing this method, we have investigated lasing properties of five NWs under forward cutting procedure. Similarly, the lasing wavelength approximately equals to the PL center wavelength for each experiment, and the observed maximum deviation of these is 4 nm. Figure 3e shows the linear relationship of the lasing wavelength and the PL center wavelength at different cut points, which may allow for the realization of precise wavelength selection in nanoscale lasers. Moreover, multiple color lasers can be obtained by selecting several NWs from one batch and cutting them to different length. For example, as shown in Supporting Information Figure S4, when we cut three NWs from the same batch, three different wavelength lasers are achieved simultaneously.

Furthermore, we find *FSR* and modes of the bandgap-graded NW lasers can be controlled through backward cutting while the dominant lasing peak is fixed at the center wavelength of the PL from the narrow-bandgap end. For example, we cut a NW of ~450 nm in diameter, ~180 μm in length from wide-bandgap end (backward cutting) step-by-step and excite the segment II: narrow-bandgap segment (Figure 4a). With a decrease of the NW length, *FSR* increases while the dominant wavelength almost stays constant at 650 nm (variation of less than 1.5 nm, Figure 4b). For a FP cavity, the *FSR* is given by an approximate expression:[35] $FSR = \lambda^2/2n_gL$, where L is the cavity length, and n_g is the effective group index of refraction at wavelength λ. *FSR* of different-length NW laser after backward cutting in Figure 4b are plotted in Figure 4c as a function of inverse NW length. As expected, there is a good linear relationship between *FSR* and 1/*L*, indicating the well-defined cavity properties originated from the reflection at the two end-facets of the NWs after cutting. The n_g is calculated to be 5.9 from the slope of the fit, which is consistent with the previously reported values.[36] By further backward cutting the NW, we have even realized single-mode lasing. As shown in Figure 4d, the laser output shows a good single-mode property with a side-mode suppression ratio of up to 14.0 dB, resulting from the strong mode competition and increase in *FSR*.[37]

From the above analysis, it can be seen that the lasing wavelength of bandgap-graded NW is determined by the center wavelength of the PL from the narrow-bandgap end, no matter how and to what length the NW was cut. This unique property

dx.doi.org/10.1021/nl500432m | *Nano Lett.* 2014, 14, 3153−3159

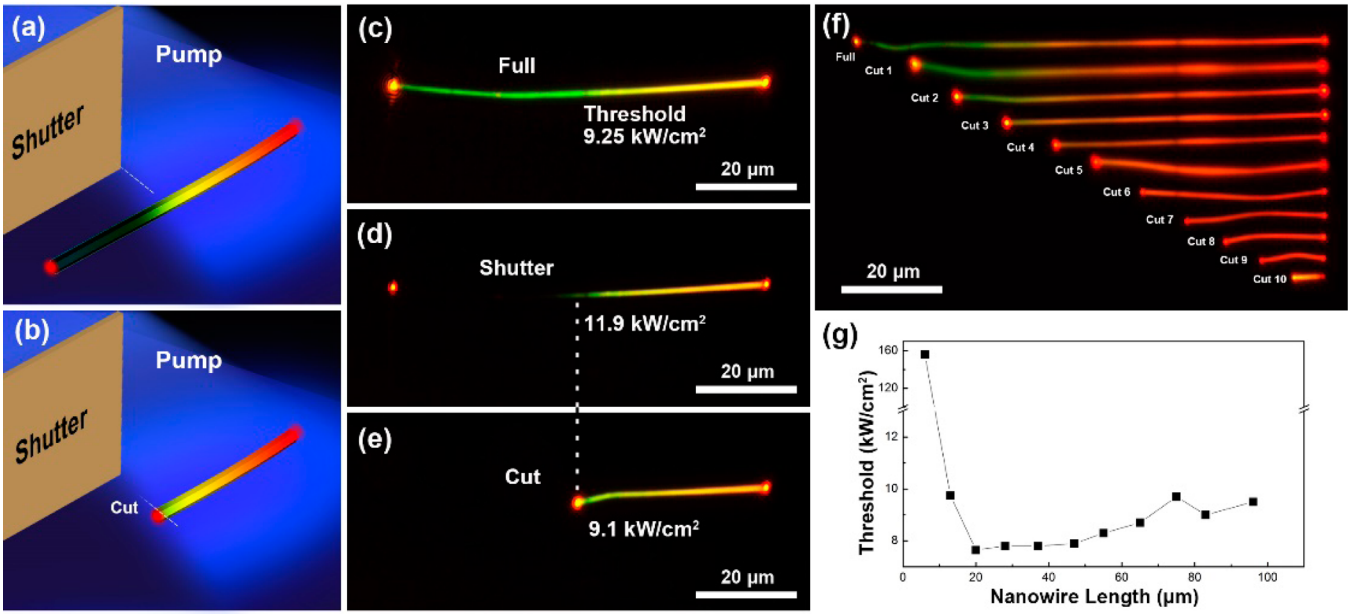

Figure 5. Investigation of threshold and gain properties of bandgap-graded NWs. (a) Schematic of a full-pumped NW blocked partly from wide-bandgap end by a shutter. (b) Schematic of a NW with cutting the segment that is blocked. (c) Real color image of a NW (~450 nm in diameter, 72 μm in length) that is fully pumped. (d) Real color image of the same NW with the left half of it (wide-bandgap section) is blocked by a shutter. (e) Real color image of the same NW with the blocked section removed. (f) Real color images of a NW (~450 nm in diameter, 98 μm in length) under a backward cutting process step-by-step. (g) Corresponding threshold recorded from each situation as a function of the NW length.

may be attributed to two main factors, which ensures the control of wavelengths in combination with modes over a wide wavelength range. First, because the wide-bandgap end of the NW is transparent to the light emitted at the narrow-bandgap end, long wavelength light is easier to reach the threshold and starts lasing.[36,38] Meanwhile, short wavelength light emitted at wide-bandgap end will experience strong bandgap absorption in the narrow-bandgap end and is very difficult to lase. The above asymmetric bandgap absorption frames the lasing wavelength in the PL range of narrow-bandgap end. Second, the lasing wavelength is fixed at the center of the PL spectrum without obvious length dependent red shifts/blue shifts resulting from the less influence of the band-tail-absorption.

The energy diagram of undoped CdSe NWs and bandgap-graded NWs are shown in Supporting Information Figure S6. The band tail of bandgap-graded NWs is likely to be larger than that of the undoped CdSe NWs. However, the influence of band-tail absorption of the wide-bandgap end on the narrow-bandgap end emission is reduced because of the gradual increase in the bandgap. The phenomena is also reported in previous work.[38] Thus, the band-tail absorption exerts a small effect on narrow-bandgap end emission of a bandgap-graded NW. On the other hand, if light is emitted from the wide-bandgap end, the bandgap absorption and band-tail-absorption of bandgap-graded NWs are significant and much larger than that of undoped NWs. No lasing is observed even when we increase the pump intensity by a factor of 100 (Supporting Information Figure S8).

In order to investigate the threshold and gain properties of these bandgap-graded NWs and understand the physical mechanism, we designed another series of experiments. Here, we use a shutter to block the light partially and compared the results with cutting process. The results are shown in Figures 5 and Supporting Information Figure S7. It is found that the threshold increases when half of the NW is not illuminated. Also, the threshold decreases a little when half of the NW is cut. It could be deduced that the wide-bandgap end may contribute to lasing accompanied by two contrasting effects: loss and gain effect. When we block the light illuminating on the wide-bandgap end, the gain effect vanishes and the loss effect dominates. The threshold increases. On the other hand, when we cut the NW, the loss effect and the gain effect vanish together. A small decrease of the threshold indicates the loss effect of the wide-bandgap end is a little larger than the gain effect. The measured slow decrease of the threshold when we backward cut the long NW step-by-step in Figure 5g (from NW length 98 to 20 μm) verify the prediction here.

The above phenomena imply that the gain properties of the bandgap-graded NWs under excitation is different from the undoped NWs, in which all the material under excitation would contribute to gain and the gain length equals to the diameter of the pump area. However, in the bandgap-graded NW lasers, the contribution of wide-bandgap end and narrow-bandgap differs a lot.

For understanding the unique gain properties of bandgap-graded NWs, we measure the length of the effective gain materials (the path length over which light intensity is amplified) of the bandgap-graded NWs. We cut the NW from wide-bandgap end to narrow-bandgap end step-by-step, which makes sure the gain material is the same during the cutting process. As shown in Figure 5f and g, the threshold gradually decreases when the length of the NW decreases from 98 to 20 μm, indicating that the sections being cut offer more loss than gain. When the length of the NW is shorter than 20 μm, the corresponding threshold increases sharply and significantly. The trend of the threshold change indicates a length of effective gain materials of ~20 μm. Several other NWs reveal similar behavior but different lengths. It is noted that the length of the effective gain material is related to the distribution of bandgap for a special NW. The threshold change trends in

dx.doi.org/10.1021/nl500432m | Nano Lett. 2014, 14, 3153−3159

the forward cutting process and in the shuttering process confirm our prediction. In both processes, the threshold increases dramatically when the pump length is smaller than the effective gain materials length (Figure 3d and Supporting Information Figure S7). The fluctuation of the threshold in forward cutting may be introduced by the fluctuation of the slope of the bandgap change.

In summary, we demonstrate NW lasers with controlling of emission wavelengths in combination with modes in individual bandgap-graded CdSSe NWs. By forward cutting, we can select and design the lasing wavelength conveniently over a wide visible range (up to 119 nm). By backward cutting, *FSR* and modes can be controlled to realize single-mode lasing. The lasing wavelength in this class of NWs is found to be determined by the center wavelength of the PL from the narrow-bandgap end and shows no obvious length-dependent red shift/blue shift. Careful analysis indicates that the lasing wavelength range is roughly framed by asymmetric bandgap absorption and the dominant lasing peak is fixed near the center wavelength of the PL from the narrow-bandgap end due to small influence of the band-tail-absorption. The investigation and measurement of the length of effective gain material in bandgap-graded NWs provides further understanding of the relationship between materials and lasing action, which indicates the gain and loss properties of bandgap-graded NWs is intrinsically different from those of the homogeneous NWs. Owing to these unique properties, the wavelengths and modes both controlled NW lasers may have many unique applications in the fields such as solid-state lighting, multicolor display, biomedical analysis, optical communication, and so forth.

■ ASSOCIATED CONTENT

Supporting Information

Additional figures and information. This material is available free of charge via the Internet at http://pubs.acs.org.

■ AUTHOR INFORMATION

Corresponding Author

*E-mail: (Q. Y.) qingyang@zju.edu.cn.

Author Contributions

[§]Z.Y. and D.W. contributed equally to this work.

Notes

The authors declare no competing financial interest.

■ ACKNOWLEDGMENTS

We thank Professor Limin Tong for his great help in experiments and discussions. We thank Pengfei Xu, Zhifang Hu, Xing Lin, Yingxin Xu, Minghua Zhuge and Xin Guo for the help in spectra measurements and Pan Wang, Fuxing Gu, Huakang Yu, Yize Lu, Dr. Wei Fang, and Professors Anlian Pan and Cunzheng Ning for helpful discussions. This work is supported by National Key Basic Research Program of China (No. 2013CB328703), National Natural Science Foundation of China (No. 51372220, 61177062, 61125402, and 51172004), the Program for Zhejiang Leading Team of S&T Innovation, and the Fundamental Research Funds for the Central Universities. T.H. acknowledges support from the Royal Academy of Engineering (Graphlex).

■ REFERENCES

(1) Lieber, C. M. *MRS Bull.* **2003**, *28*, 486−491.
(2) Yan, R.; Gargas, D.; Yang, P. *Nat. Photonics* **2009**, *3*, 569−576.
(3) Zimmler, M. A.; Bao, J.; Capasso, F.; Müller, S.; Ronning, C. *Appl. Phys. Lett.* **2008**, *93*, 051101.
(4) Ma, Y.; Guo, X.; Wu, X.; Dai, L.; Tong, L. *Adv. Opt. Photonics* **2013**, *5*, 216−273.
(5) Piccione, B.; Cho, C.-H.; van Vugt, L. K.; Agarwal, R. *Nat. Nanotechnol.* **2012**, *7*, 640−645.
(6) Huang, M. H.; Mao, S.; Feick, H.; Yan, H.; Wu, Y.; Kind, H.; Weber, E.; Russo, R.; Yang, P. *Science* **2001**, *292*, 1897−1899.
(7) Johnson, J. C.; Choi, H.-J.; Knutsen, K. P.; Schaller, R. D.; Yang, P.; Saykally, R. J. *Nat. Mater.* **2002**, *1*, 106−110.
(8) Duan, X.; Huang, Y.; Agarwal, R.; Lieber, C. M. *Nature* **2003**, *421*, 241−245.
(9) Gradečak, S.; Qian, F.; Li, Y.; Park, H.-G.; Lieber, C. M. *Appl. Phys. Lett.* **2005**, *87*, 173111.
(10) Pauzauskie, P. J.; Sirbuly, D. J.; Yang, P. *Phys. Rev. Lett.* **2006**, *96*, 143903.
(11) Hua, B.; Motohisa, J.; Kobayashi, Y.; Hara, S.; Fukui, T. *Nano Lett.* **2008**, *9*, 112−116.
(12) Saxena, D.; Mokkapati, S.; Parkinson, P.; Jiang, N.; Gao, Q.; Tan, H. H.; Jagadish, C. *Nat. Photonics* **2013**, *7*, 963−968.
(13) Mayer, B.; Rudolph, D.; Schnell, J.; Morkotter, S.; Winnerl, J.; Treu, J.; Muller, K.; Bracher, G.; Abstreiter, G.; Koblmuller, G.; Finley, J. J. *Nat. Commun.* **2013**, *4*, 2931.
(14) Ding, Y.; Yang, Q.; Guo, X.; Wang, S.; Gu, F.; Fu, J.; Wan, Q.; Cheng, J.; Tong, L. *Opt. Express* **2009**, *17*, 21813−21818.
(15) Yang, Q.; Jiang, X.; Guo, X.; Chen, Y.; Tong, L. *Appl. Phys. Lett.* **2009**, *94*, 101108.
(16) Hänsch, T. W.; Shahin, I.; Schawlow, A. *Phys. Rev. Lett.* **1971**, *27*, 707−710.
(17) Pascu, M.; Moise, N.; Staicu, A. *J. Mol. Struct.* **2001**, *598*, 57−64.
(18) Buus, J.; Murphy, E. J. *J. Lightwave Technol.* **2006**, *24*, 5−11.
(19) Xiao, Y.; Meng, C.; Wang, P.; Ye, Y.; Yu, H.; Wang, S.; Gu, F.; Dai, L.; Tong, L. *Nano Lett.* **2011**, *11*, 1122−1126.
(20) Qian, F.; Li, Y.; Gradecak, S.; Park, H. G.; Dong, Y. J.; Ding, Y.; Wang, Z. L.; Lieber, C. M. *Nat. Mater.* **2008**, *7*, 701−706.
(21) Pan, A.; Zhou, W.; Leong, E. S.; Liu, R.; Chin, A. H.; Zou, B.; Ning, C. *Nano Lett.* **2009**, *9*, 784−788.
(22) Liu, Y. K.; Zapien, J. A.; Shan, Y. Y.; Geng, C. Y.; Lee, C. S.; Lee, S. T. *Adv. Mater.* **2005**, *17*, 1372−1377.
(23) Liu, Y. K.; Zapien, J. A.; Shan, Y. Y.; Tang, H.; Lee, C. S.; Lee, S. T. *Nanotechnology* **2007**, *18*, 365606.
(24) Li, J.; Meng, C.; Liu, Y.; Wu, X.; Lu, Y.; Ye, Y.; Dai, L.; Tong, L.; Liu, X.; Yang, Q. *Adv. Mater.* **2013**, *25*, 833−837.
(25) Liu, X.; Zhang, Q.; Xiong, Q.; Sum, T. C. *Nano Lett.* **2013**, *13*, 1080−1085.
(26) Liu, X.; Zhang, Q.; Yip, J. N.; Xiong, Q.; Sum, T. C. *Nano Lett.* **2013**, *13*, 5336−5343.
(27) Gu, F.; Yang, Z.; Yu, H.; Xu, J.; Wang, P.; Tong, L.; Pan, A. *J. Am. Chem. Soc.* **2011**, *133*, 2037−2039.
(28) Yang, Z.; Xu, J.; Wang, P.; Zhuang, X.; Pan, A.; Tong, L. *Nano Lett.* **2011**, *11*, 5085−5089.
(29) Zhuang, X.; Ning, C. Z.; Pan, A. *Adv. Mater.* **2012**, *24*, 13−33.
(30) Li, L.; Lu, H.; Yang, Z.; Tong, L.; Bando, Y.; Golberg, D. *Adv. Mater.* **2013**, *25*, 1109−1113.
(31) Lu, Y.; Gu, F.; Meng, C.; Yu, H.; Ma, Y.; Fang, W.; Tong, L. *Opt. Express* **2013**, *21*, 22314−22319.
(32) Xu, J.; Zhuang, X.; Guo, P.; Huang, W.; Hu, W.; Zhang, Q.; Wan, Q.; Zhu, X.; Yang, Z.; Tong, L.; Duan, X.; Pan, A. *Sci. Rep.* **2012**, *2*, 820.
(33) Tong, L.; Lou, J.; Gattass, R. R.; He, S.; Chen, X.; Liu, L.; Mazur, E. *Nano Lett.* **2005**, *5*, 259−262.
(34) Tong, L.; Gattass, R. R.; Ashcom, J.; He, S.; Lou, J.; Shen, M.; Maxwell, I.; Mazur, E. *Nature* **2003**, *426*, 816−819.
(35) Siegman, A. E. *Lasers*; Oxford University Press: Oxford, U. K., 1986.
(36) Liu, Z.; Yin, L.; Ning, H.; Yang, Z.; Tong, L.; Ning, C.-Z. *Nano Lett.* **2013**, *13*, 4945−4950.

(37) Li, Q.; Wright, J. B.; Chow, W. W.; Luk, T. S.; Brener, I.; Lester, L. F.; Wang, G. T. *Opt. Express* **2012**, *20*, 17873−17879.
(38) Guo, P.; Zhuang, X.; Xu, J.; Zhang, Q.; Hu, W.; Zhu, X.; Wang, X.; Wan, Q.; He, P.; Zhou, H.; Pan, A. *Nano Lett.* **2013**, *13*, 1251−1256.